Energy Extraction Efficiency

Yanran Xia

Philippe Rochefort

Prof. Guy Dumas

Two simplified models for numerical turbine array simulations

Who should read this paper?

The contributions presented in this paper are valuable for researchers and practitioners researching reliable methods for analyzing turbine layout performance during the design phase of hydrokinetic turbine farms; for researchers interested in wake-turbine interactions; and for Computational Fluid Dynamics (CFD) specialists interested in hydrokinetic and wind turbine modelling.

Why is it important?

This work presents the first direct comparison of two simplified turbine models based on volumetric force-prediction techniques, namely the Effective Performance Turbine Model and the Actuator Line Method, for multi-turbine configurations. These models not only make such farm analysis computationally feasible compared to high-fidelity blade-resolved simulations, they also provide accurate performance and wake predictions for array-scale analysis.

This paper also provides new physical insights for tandem and clustered turbine arrangements – configurations that remain sparsely documented in the literature. The strengths and limitations of each approach are evaluated, leading to recommendations on their appropriate use depending on the turbine array configuration.

As the ocean will increasingly host larger turbine farms, modelling tools that are both accurate and computationally efficient will be needed to support the planning, the optimization, and the environmental assessment for turbine array deployment.

About the authors

Yanran Xia is a PhD candidate at the CFD laboratory LMFN at Université Laval. Her research focuses on numerical modelling of hydrokinetic turbines and optimization of turbine farm deployment in marine environments. Her expertise includes fluid mechanics and CFD. She has experience working with CFD solvers such as Star-CCM+.

Philippe Rochefort is an M.Sc. candidate at the CFD laboratory LMFN at Université Laval with expertise in fluid mechanics and CFD, particularly using Star-CCM+. His research focuses on the modelling of vertical-axis turbines using the Actuator Line Method, aiming to improve performance prediction under realistic conditions while reducing computational cost.

Prof. Guy Dumas is a professor as well as the founder and director of the CFD laboratory LMFN at Université Laval, where he specializes in aero-hydrodynamics and numerical simulations. He investigates vortical and turbulent flows to shed light on the complex physics of fluid-structure interactions and to optimize systems of renewable energy production. His group has contributed to advancing hydrokinetic turbine technologies and developing various concepts of oscillating-foils turbine.

COMPARISON OF TWO SIMPLIFIED MODELS FOR NUMERICAL TURBINE ARRAY SIMULATIONS

Yanran Xia, Philippe Rochefort, Guy Dumas*
CFD Laboratory LMFN, Department of Mechanical and Industrial Engineering, Université Laval, Québec, QC, Canada
**Corresponding author: guy.dumas@gmc.ulaval.ca*
DOI: https://doi.org/10.48336/TMT0-7G93

ABSTRACT

To improve the energy extraction efficiency of hydrokinetic turbine farms, it is necessary to study the performance of different turbine array configurations. However, predicting and analyzing the performance of turbine arrays using high-fidelity blade-resolved simulations is unrealistic due to excessive computational cost. A solution to reduce computational demand while maintaining realistic performance predictions and accurate representation of flow physics is to use simplified turbine models. This work presents a comparison between two simplified modelling approaches developed at Université Laval for cross-flow turbines of the H-Darrieus type: the Actuator Line Method (ALM) and the Effective Performance Turbine Model (EPTM). Both approaches consist of representing the real rotor by equivalent volumetric forces, thus bypassing the resolution of the blades and their boundary layers. The ALM is an unsteady method that requires the computation, at each time step, of the force distribution to be applied along the span of the turbine's blades. Thus, this method accurately reproduces the local impact of the blade on the flow field and to generate realistic near-wake structures. On the other hand, the steady-state EPTM imposes time-averaged blade forces within an annular cylindrical actuating region to reproduce the mean effects of the rotor on the flow, which predicts the mean turbine performance and generates a reasonably accurate mean wake. Compared to the EPTM, the ALM is of higher fidelity, capturing more physical details, but computationally more expensive.

Three turbine configurations (single turbine, tandem array, and triangular cluster) are simulated using both approaches. The two methods are evaluated and compared in terms of the prediction of key performance metrics (i.e., power and drag coefficients) and in terms of their wake reproduction capability. Recommendations for turbine farm analysis are formulated.

Keywords: Hydrokinetic energy, cross-flow turbine, turbine arrays, simplified modelling, actuator line, actuator disk

1. INTRODUCTION

Hydrokinetic turbines are technologies that allow the extraction of kinetic energy from freestream water flows, such as river and tidal currents, in a manner analogous to wind turbines. This work focuses on the H-Darrieus Cross-Flow Turbine (CFT) technology, which is composed of straight blades rotating at a constant radius along the entire span. The CFTs, deployed vertically, are well adapted to the bi-directional or multi-directional tidal flows. They can also be deployed horizontally in shallow water applications where their rectangular extraction plane allows to maximize the power. Thus, their adaptability to different environments and their ease of installation [1], [2] make them advantageous compared to axial-flow turbines. In this work, we consider CFTs deployed vertically.

Deploying these turbines in arrays or farms becomes an interesting option to minimize installation and maintenance costs while maximizing energy extraction on regional scales. Dabiri [3] also demonstrated in 2011 that the energy density of turbine farms is increased when using CFTs compared to axial-flow turbine farms, which makes this technology even more attractive for farm-scale deployment.

The main challenges when considering turbine farms are related to total power prediction and configuration optimization. Hydrokinetic turbine arrays are not simple superposition of isolated turbines; instead, complex interactions exist among turbines, such as the local blockage effects caused by closely placed side-by-side turbines [4], [5], as well as the impact of upstream wakes on downstream turbines [5], [6], [7]. Moreover, resource-related factors – such as the global blockage induced by the channel bed and the free surface [8], [9], free surface deformation [6], and inflow characteristics [10], [11], [12] – also have a significant influence on the array performance. Therefore, it is essential to account for these aspects in turbine array studies.

During the design phase of turbine farms, Computational Fluid Dynamics (CFD) is an important tool to assess the array performance and optimize the turbine layout. High-fidelity Blade-Resolved (BR) simulations are often applied for the performance and wake characterization of single turbines [13], [14], [15]. However, BR simulations are highly demanding in computational cost due to the boundary layers resolution near the solid bodies. As a result, using BR simulations for configuration with multiple turbines becomes unrealistic due to the excessive computational cost. A solution to reduce computational demands while still providing reliable predictions is to use simplified turbine models, such as force prediction-based modelling techniques like the Effective Performance Turbine Model (EPTM) [16] and the Actuator Line Method (ALM) [17]. These two simplified approaches, which have been adapted for CFTs at Université Laval, are used in this study.

This work thus aims to compare these two simplified models adapted to the turbine geometry described in Section 2.1 based on their performance predictions, wake reproduction, and computational costs for three deployment scenarios: single turbine and

two different multi-turbine configurations. The modelling details of both approaches are presented in Sections 2.2 and 2.3, while the results for the three configurations (single turbine, tandem array, and triangular cluster) are discussed in Section 4. Finally, recommendations for the analysis of turbine farms using these two simplified models are provided in order to highlight the advantages and limitations of each approach and to address the following question: Which model is best suited to optimize turbine farm configurations?

2. TURBINE MODELLING

As mentioned earlier, resolving boundary layers in BR simulations requires a very fine computational mesh near solid bodies to capture the strong normal gradient of velocity, which significantly increases the computational cost. The simplified models EPTM and ALM presented in this work are both actuator-type turbines models, which replace solid bodies with actuating regions in which estimated volumetric forces are imposed. As a result, boundary layer resolution is bypassed in these models, which reduces computational cost while still maintaining accurate performance predictions.

This section first presents the reference turbine, along with the normalized parameters that typically characterize CFTs. Then, the general working principles of the two simplified models EPTM and ALM are described.

2.1 Description of the Reference Turbine

The reference turbine, shown in Figure 1, consists of a three-bladed CFT with a simplified cylindrical hub, originally designed and tested by Mavi Innovations. Supporting struts and foundation structures are not considered for simplification purpose. Detailed parameters of geometric characteristics and operating conditions are presented in Table 1. In this study, the turbine operates always at its rotational speed corresponding to its optimal power extraction point whatever its deployment conditions. The tip-speed ratio is a normalized value of the rotational speed Ω, defined as:

$$\lambda \equiv \Omega R / U_{\infty}, \tag{1}$$

where $R \equiv D/2$ is the rotor radius and U_{∞} is the freestream velocity. The optimal tip-speed ratio (λ_{opt}) of a specific turbine design varies depending on the blockage ratio:

$$B = A / A_{\mathrm{channel}}, \tag{2}$$

where $A = bD$ is the turbine's frontal area and A_{channel} is the cross-sectional area of the channel. For the investigated CFT, the optimal tip-speed ratio is of 3 in a confined environment with a blockage ratio of 20% [18]. The diameter-based rotor Reynolds number is fixed at $Re_D \equiv U_{\infty} D/\nu = 1.07 \cdot 10^7$ (with ν being the fluid kinematic viscosity), which is high enough to assume Reynolds independence [19] and fully turbulent boundary layers.

Conventional turbine performance metrics include several non-dimensional parameters, such as the mean power coefficient, defined as the ratio of time-averaged (mean) power extraction ($\overline{P}$) to the available power across the turbine's extraction window:

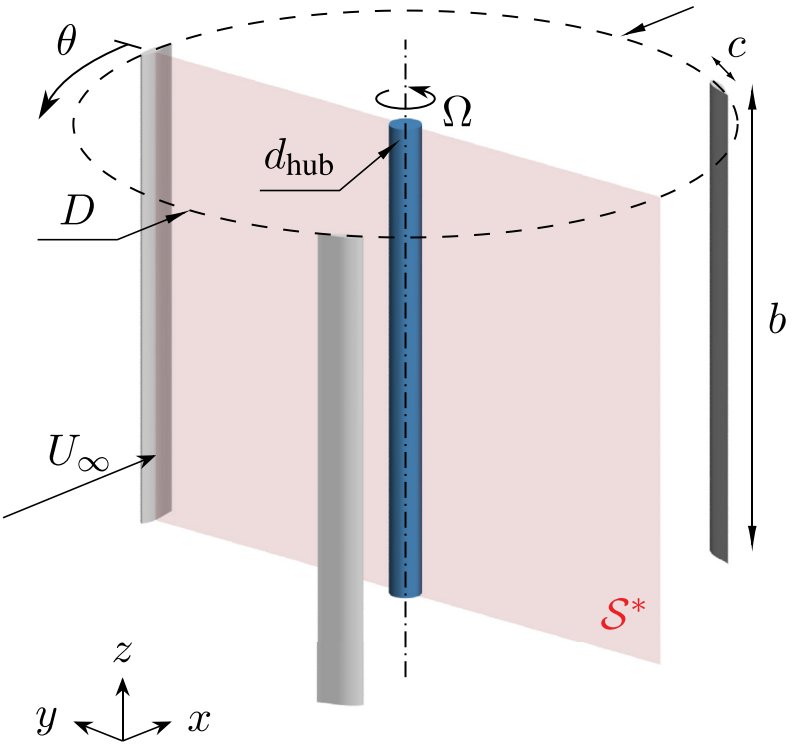

Figure 1: Three-bladed turbine geometry and main parameters.

Table 1: Main normalized geometric and operational characteristics of the reference turbine.

Parameter	Symbol	Value
Turbine geometry		
Blade number		3
Blade profile		NACA 63-021
Blade span	b/D	0.75
Blade chord	c/D	1/14
Blade attachment point	x_p/c	0.25
Blade pitch angle	β	0°
Hub diameter	d_{hub}/D	0.05
Operating conditions		
Blockage ratio	B	20%
Tip-speed ratio design	λ	3
Rotor Reynolds number	Re_D	1.07×10^7
Blade Reynolds number	$Re_c = (\Omega R)c/\nu$	2.29×10^6

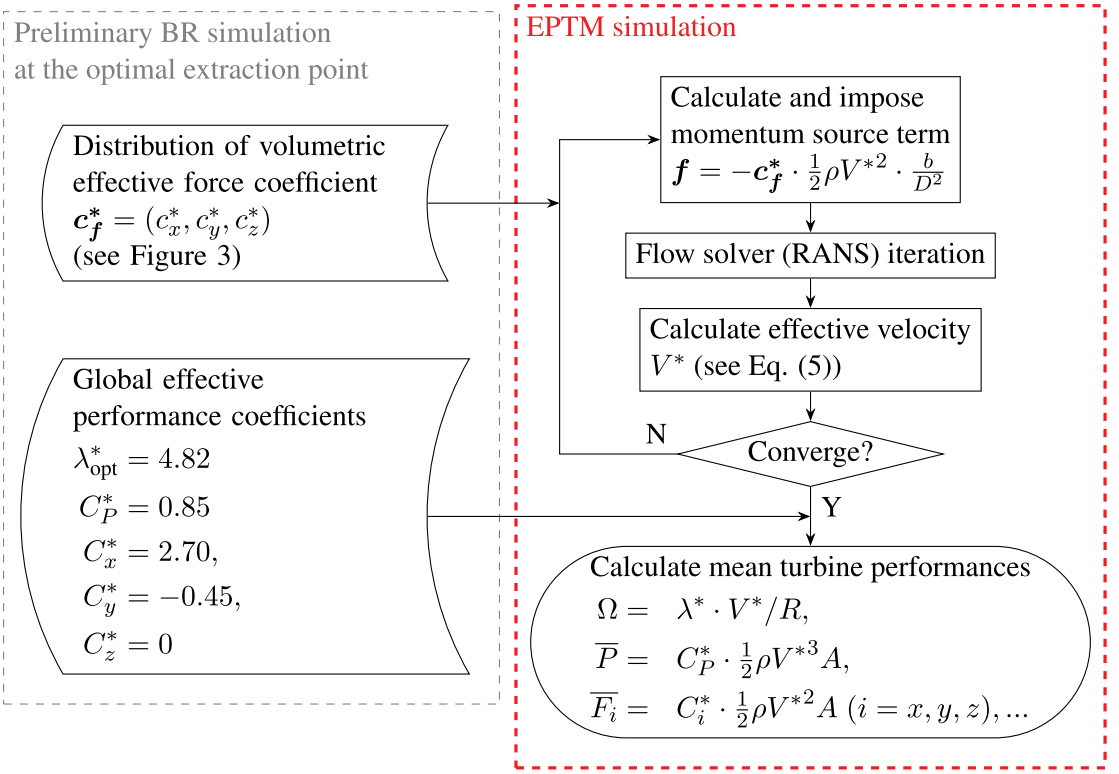

Figure 2: Overall computational workflow of an Effective Performance Turbine Model (EPTM) simulation.

$$\overline{C_P} \equiv \frac{\overline{P}}{\frac{1}{2}\rho U_\infty^3 A}, \tag{3}$$

and the mean drag coefficient (also referred to as the mean thrust coefficient), defined as a normalized value of the drag force, i.e., the mean streamwise force acting on the turbine ($\overline{F_x}$):

$$\overline{C_x} \equiv \frac{\overline{F_x}}{\frac{1}{2}\rho U_\infty^2 A}, \tag{4}$$

where ρ is the fluid density.

2.2 Low-fidelity Simplified Turbine Model: EPTM

The EPTM is a steady-state simplified turbine model for use in a three-dimensional Reynolds-Averaged Navier-Stokes (RANS) CFD simulation of the deployment site, originally developed at Université Laval by Bourget in 2018 [16], which has been specially formulated for the reference CFT considered here and further validated and applied under various operating environments [20]. As an actuator-disk type model, the EPTM imposes volumetric forces (i.e., momentum source terms in the RANS equation) directly into the fluid domain to mimic the time-averaged impact of the real turbine. The cylindrical actuating region replicates the geometry of the CFT's blades swept area. This approach avoids not only the resolution of boundary layers but also the long temporal resolution.

Figure 2 presents the overall calculation process of an EPTM simulation. The key feature of EPTM is that the applied volumetric forces *f* and the mean performance metrics

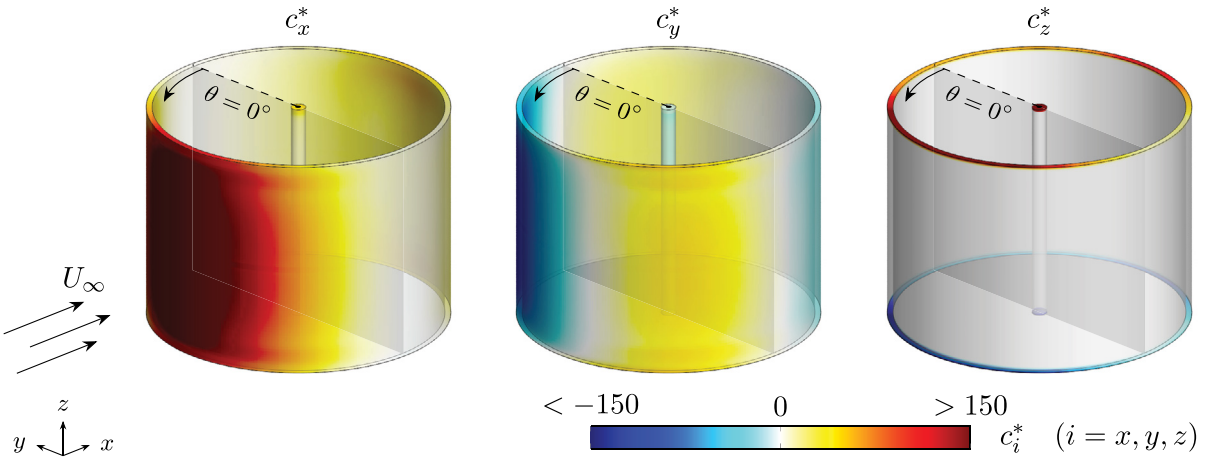

Figure 3: Distribution of the streamwise (c_x^*), transverse (c_y^*), and axial (c_z^*) components of the volumetric effective force coefficient c_f^*. The transparent grey plane denotes the turbine extraction plane.

(e.g., the optimal rotational speed Ω, the mean output power $\overline{P}$, and the mean drag force $\overline{F}_x$) are all scaled with the effective velocity V^*, which is defined as the time- and space-averaged velocity passing through the rotor (see the pink plane denoted S^* in Figure 1):

$$V^* \equiv Q/A \tag{5}$$

with Q being the mean flowrate through the rotor. This effective velocity is not known a priori, but results from the simulation. Indeed, V^* is the main performance metric provided by the EPTM. Other performance metrics are computed from it as expressed in the chart of Figure 2. At each RANS iteration step, the effective velocity V^* is recalculated and is used to update the volumetric force f. Once the solution converges, final prediction of the mean turbine performance can be derived. It is important to note that the input data, i.e., the distribution of the volumetric effective force coefficient (c_f^*) illustrated in Figure 3, as well as the global effective coefficients, including the effective tip-speed ratio (λ^*), the effective power coefficient (C_P^*), and the effective force coefficients ($C_{x,y,z}^*$) are all extracted from a preliminary BR simulation of an isolated turbine at its optimal extraction point. Note that the global mean force $\overline{F_{x,y,z}}$ are the volume integrals over the actuating region of the components of f in their corresponding directions [16].

Since the effective velocity V^* represents the local flow "effectively experienced" by the turbine, the EPTM is intrinsically able to account for the rotor-scale local flow effects such as the blockage effect and velocity variations in the upstream vicinity. The former may be due to the channel confinement or the presence of neighbouring turbines while the latter may be associated to the velocity deficit produced by upstream turbines. Moreover, in all circumstances, the EPTM tracks the optimal power extraction point automatically.

2.3 Medium-fidelity Simplified Turbine Model: ALM

The ALM is a medium-fidelity and unsteady model that can be used to predict the time evolution of the performances [21], [22] and to accurately replicate the unsteady turbine wake structures due to the blade rotation

[23]. In this approach, the solid bodies, i.e., the blades and hub of the CFT, are replaced by straight actuating lines in rotation (for the blades) along which varying volumetric forces are applied into the Navier-Stokes equations, as shown in Figure 4. The actuating lines are formed with actuating points uniformly spaced in the spanwise (z) direction, and the force distribution is constructed based on the force contributions from individual point. The lift ($\Delta_p f_l$) and drag ($\Delta_p f_d$) forces for each actuating point are calculated with the estimated local flow properties [24]: the blade-scale effective local freestream velocity (V) and the effective angle of attack (α), as well as the precomputed 2D aerodynamic polars (i.e., lift and drag curves) of the blade's profile:

$$\Delta_p f_l = \frac{1}{2}\rho|\boldsymbol{V}|^2 \Delta_p A C_l(\alpha), \tag{6}$$

$$\Delta_p f_d = \frac{1}{2}\rho|\boldsymbol{V}|^2 \Delta_p A C_d(\alpha), \tag{7}$$

where $C_l(\alpha)$ and $C_d(\alpha)$ are the lift and drag coefficients corresponding to α, and $\Delta_p A = \Delta_p z \cdot c$ is the area attributed to each point. Resulting forces are implemented in the fluid domain to replicate the actual blades' effects on the flow. Since CFT blades operate in curved flow, it is necessary to apply analytical curvature corrections to the lift and drag coefficients [25] to adapt the ALM to CFT. Additionally, near-tip correction functions developed specifically for the ALM [26] are used to adapt the force loading near the blade tips, as the standard ALM struggles to accurately reproduce tip loading due to a poor representation of tip vortices. The instantaneous power coefficient (C_P) is computed using the tangential force component along the blade chord, which results from the projection of $\Delta_p f_l$ and $\Delta_p f_d$ onto the chord direction, as well as the resulting moment at the attachment point. Compared to other ALM adaptations for CFTs previously proposed in the literature [27], [28], [29], the ALM used in this work is improved through the incorporation of new analytical curvature corrections and near-tip correction functions. These enhancements maintain the simplicity of the ALM while significantly improving its predictive capabilities [17].

3. NUMERICAL SETTINGS

The EPTM, ALM, and BR simulations in this work are all performed using the finite-volume commercial CFD software Simcenter™ STAR-CCM+™ [30]. The BR simulations have been realized by Bourget [16] and Gauvin-Tremblay and Dumas [6].

Table 2 provides a summary of the general numerical setups for the two types of simplified turbine simulations and the reference BR simulations.

The EPTM simulations are conducted with the steady-state solver while the ALM and BR simulations are non-stationary with time advancing using a second-order implicit scheme. The time discretization corresponds to 1,000 time steps per turbine revolution period for unsteady simulations. (U)RANS approaches are applied to account for the turbulence with either the k-ω SST or the Spalart-Allmaras model.

Three turbine configuration scenarios are considered in this work: #1 single turbine, #2 tandem array, and #3 triangular cluster,

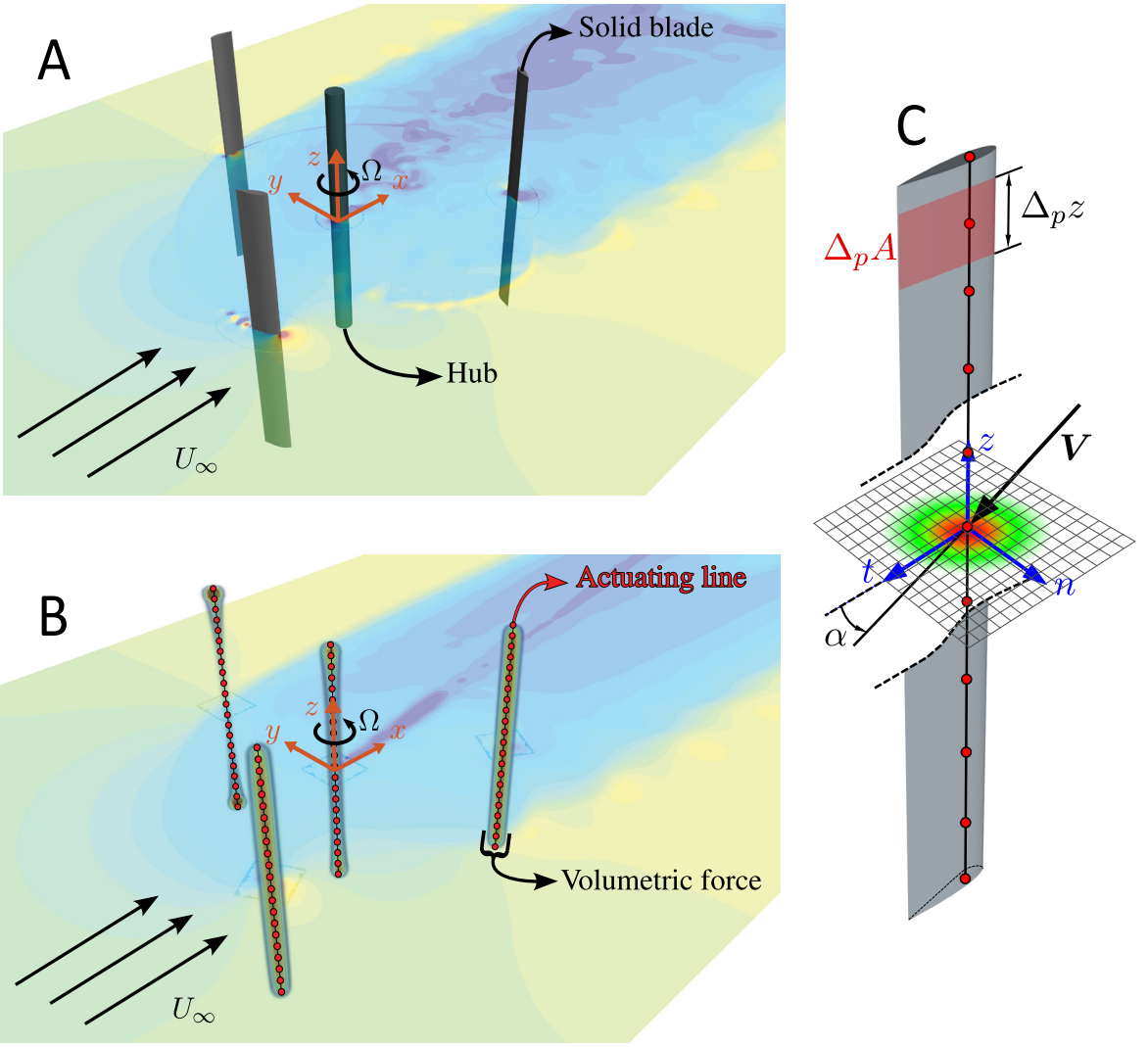

Figure 4: Comparison of (a) the actual blades of the Cross-Flow Turbine (CFT) and (b) the Actuator Line Method (ALM) representation via volume rendering of the actuating forces. The actuator line concept of a single blade is shown in (c), with the control points (in red), their associated coordinate frame (in blue), as well as the actuating force contour on a plane section passing a control point.

Table 2: Summary of numerical setups for the three types of simulations. SST = Shear Stress Transport. SIMPLE = Semi-Implicit Method for Pressure-Linked Equations.

	EPTM	ALM	BR
Solver			
Time advancement	Steady-state	Second-order implicit unsteady (1,000 steps/cycle)	
Pressure-velocity coupling	Segregated SIMPLE	Coupled	Segregated SIMPLE
Turbulence model	RANS k-ω SST	URANS Spalart-Allmaras	URANS k-ω SST
Boundary conditions			
Inlet	Uniform velocity: U_∞ Uniform low turbulence: • $\nu_t/\nu = 10$, $I = 1\%$ for k-ω SST (EPTM and BR) • $\nu_t/\nu = 0.2$ for Spalart-Allmaras (ALM)		
Outlet	Uniform static pressure: $p = 0$		
Lateral	Symmetry plane		

as illustrated in Figure 5. The computational domains are in the shape of a rectangular channel, extending at least $10D$ upstream and $15D$ downstream of the turbine (or turbine array). For the single turbine and tandem array scenarios, the cross section of the channel has the same aspect ratio as that of the turbine. The channel width is doubled for the triangular cluster scenario. The blockage ratio (see Equation (2)) based on the frontal area of one turbine for scenarios #1 and #2 and on the frontal area of two turbines for scenario #3, is always maintained at 20% in all cases. Constant and uniform inflow with low turbulence level is specified at the inlet boundary and a zero static pressure is imposed at the outlet boundary. The lateral boundaries are simplified as symmetry planes.

The overset mesh approach supported by Star-CCM+ is used here. The background channel and the inner domains, which contain the actuating regions or the rotor geometry, are meshed separately using hexahedral or polyhedral cells (as shown in Figure 6). Overset mesh technique is applied to connect the background mesh and the meshes of the inner domains. The inner mesh cells are refined to about $0.01D$ in the vicinity of the actuating region of the EPTM and ALM, which are much finer around the BR rotor geometry ($\leq 0.0025D$ and $\leq 0.005D$ for the scenario #1 and #2, respectively) with boundary layers discretized to ensure $y^+ \sim 1$. The background mesh is progressively coarsened away from the turbine surrounding regions, but a resolution not coarser than $0.05D$ is maintained up to at least

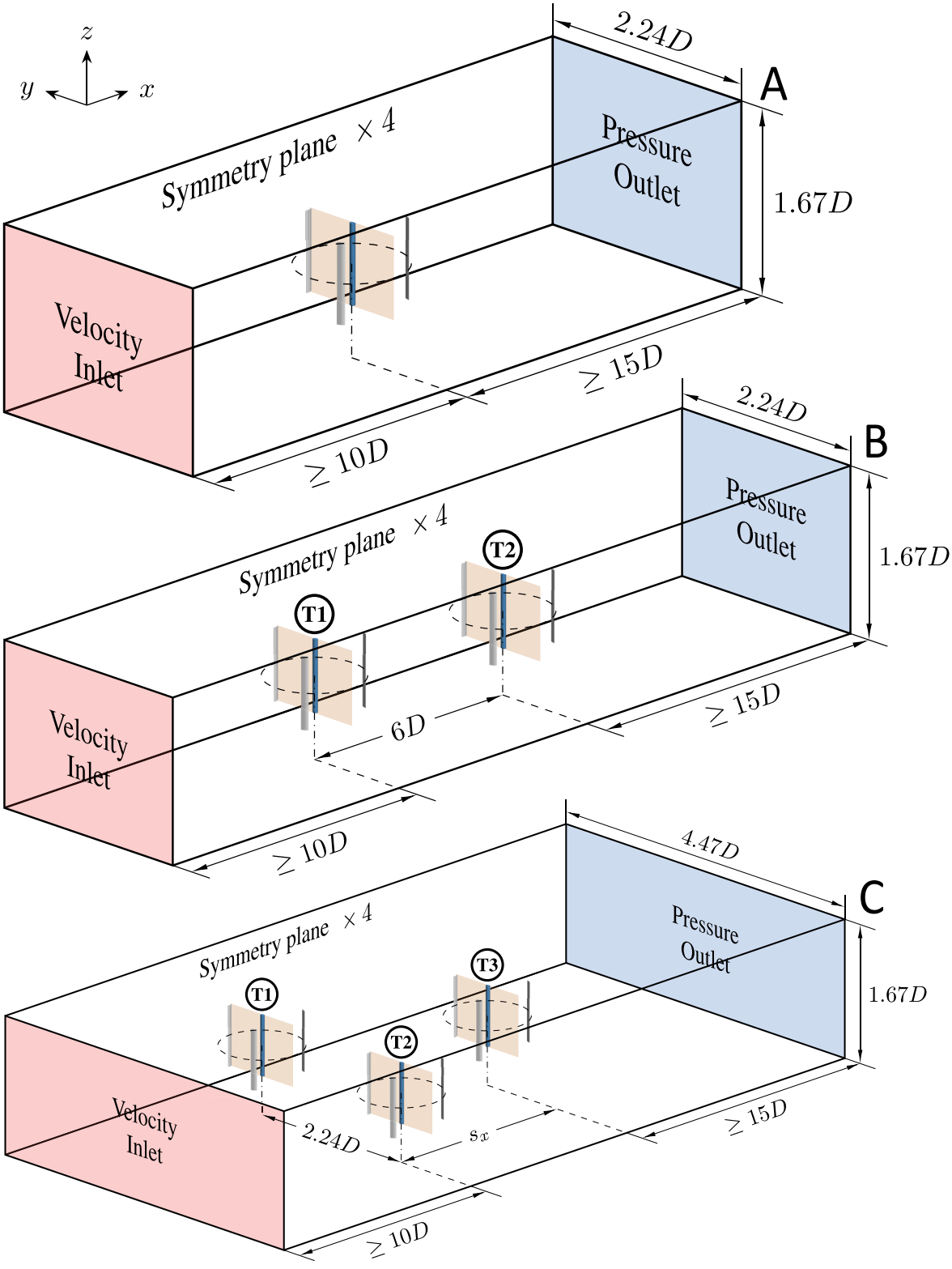

Figure 5: Geometry of the computational domain and boundary conditions for the three scenarios. The dimensions in the streamwise (x) direction are not drawn to scale for illustrative purposes. (a) Scenario #1 Single turbine. (b) Scenario #2 Tandem array. (c) Scenario #3 Triangular cluster.

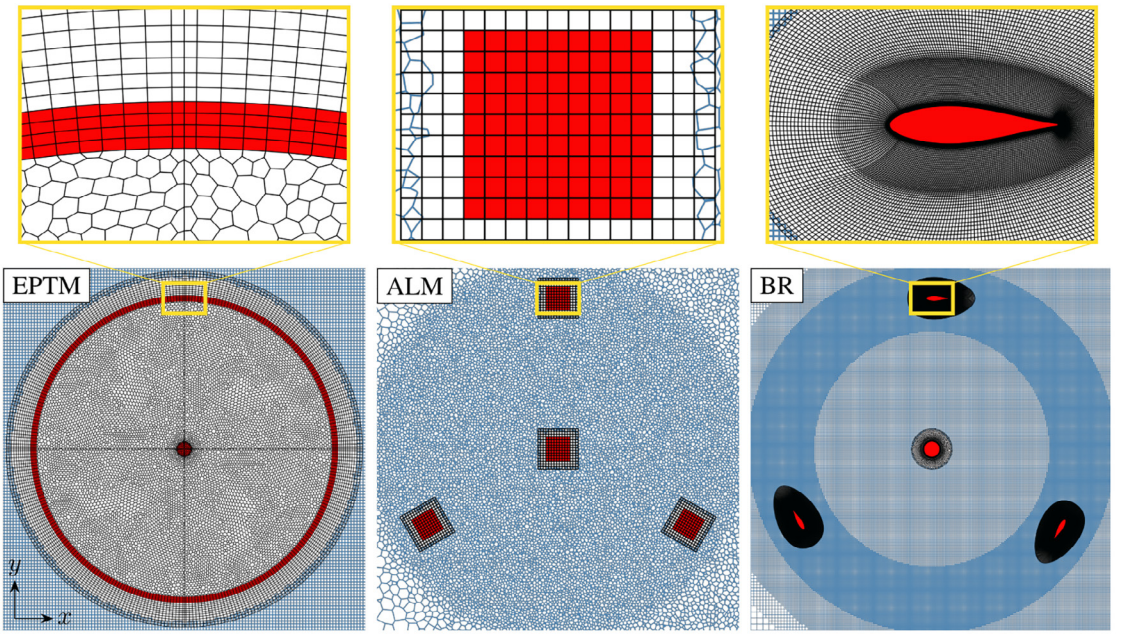

Figure 6: Illustration of the meshes around the turbine models on the mid-span horizontal plane section (at $z = 0$) for the three types of simulation. The background mesh is drawn in blue and the overset mesh is drawn in black. The actuating zones of the Effective Performance Turbine Model (EPTM) and Actuator Line Method (ALM) as well as the solid blades in the Blade-Resolved (BR) simulation are filled in red.

$7D$ downstream of the turbines to well capture the wake structures for all the simulations.

4. RESULTS AND DISCUSSION

In this section, the two simplified turbine models EPTM and ALM are compared in terms of the performance prediction, wake reproduction, and computational costs for the three investigated scenarios shown in Figure 5. High-fidelity BR simulation results are provided for the first two scenarios as reference for comparison. For the unsteady ALM and BR simulations, mean results are derived from time-averaging over at least three additional turbine revolution periods after statistical convergence, while the steady-state EPTM simulations give directly time-averaged predictions.

4.1 Scenario #1: Single Turbine

In this basic scenario, a single CFT operates in a confined environment with a blockage ratio of $B = 20\%$ (see Figure 5a).

The ALM and BR simulations are conducted at various tip-speed ratios (λ) to characterize the mean performances of the isolated turbine. The EPTM, by design, can only provide the predictions at the optimal operation point with maximum power extraction. The results are presented in Figure 7. The $\overline{C_P}$ curves (Figure 7a) show that a same optimal tip-speed ratio $\lambda_{\text{opt}} = 3$ is predicted by all the three approaches. The mean power coefficients estimated by the EPTM, which was constructed based on an unconfined BR simulation of that CFT, match well the value from the reference BR simulation carried out at the 20% confinement level. The ALM overpredicts the turbine power but within an acceptable margin (~15% in relative). As for the mean drag coefficient $\overline{C_x}$ (see Figure 7b), it is found that the three modelling approaches yield comparable

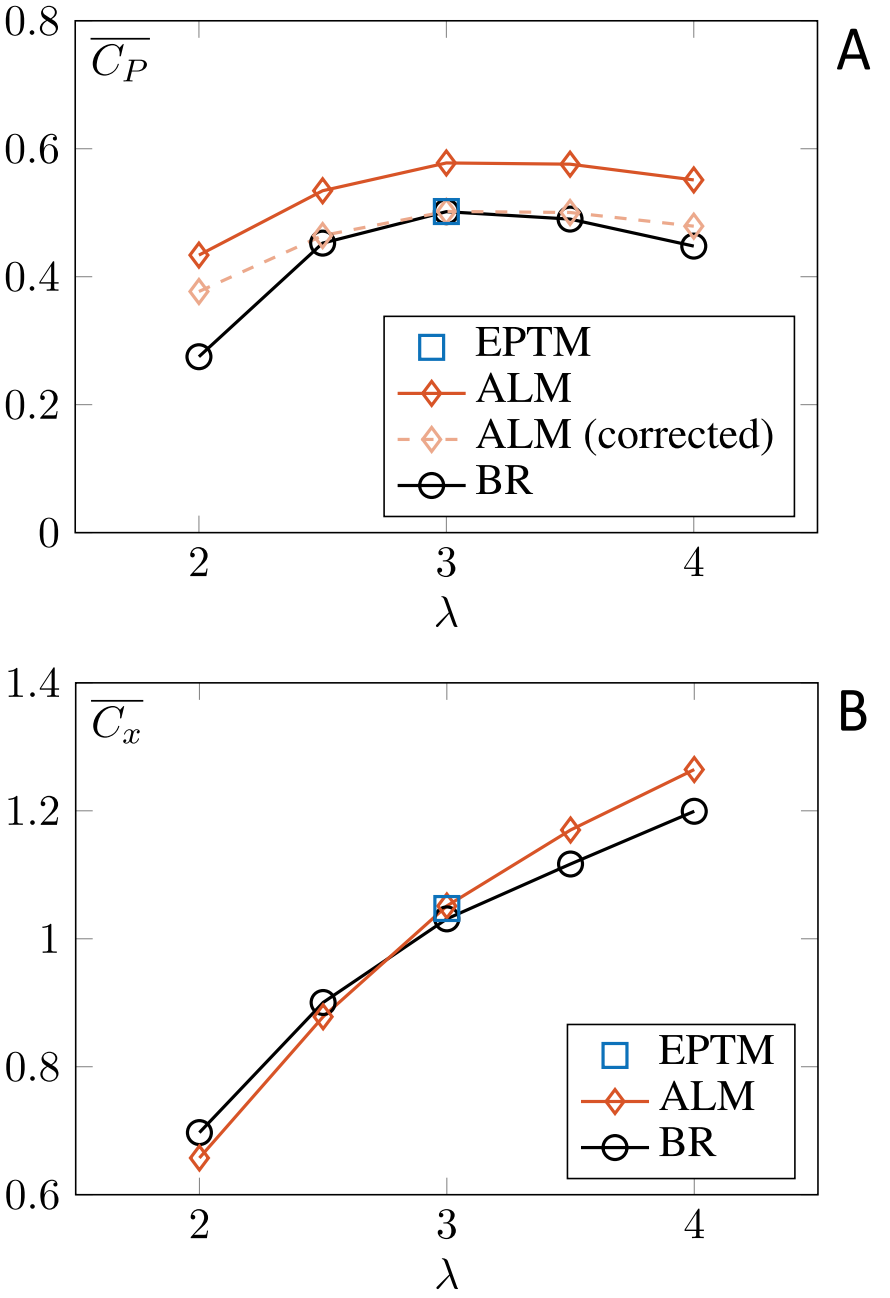

Figure 7: Mean performance curves of a single turbine at various tip-speed ratios (λ) under a fixed blockage ratio of B = 20%, predicted by different turbine modelling approaches. (a) Power coefficient. (b) Drag coefficient.

predictions with only a 2% relative difference at the optimal point, signifying that the EPTM and the ALM both exert a similar mean effect on the fluid in the streamwise direction as the BR turbine does.

The overprediction of $\overline{C_P}$ with the ALM can be explained by its poor representation of tip vortices. Figure 8a shows that the overprediction of the instantaneous power coefficient C_P of one single blade occurs

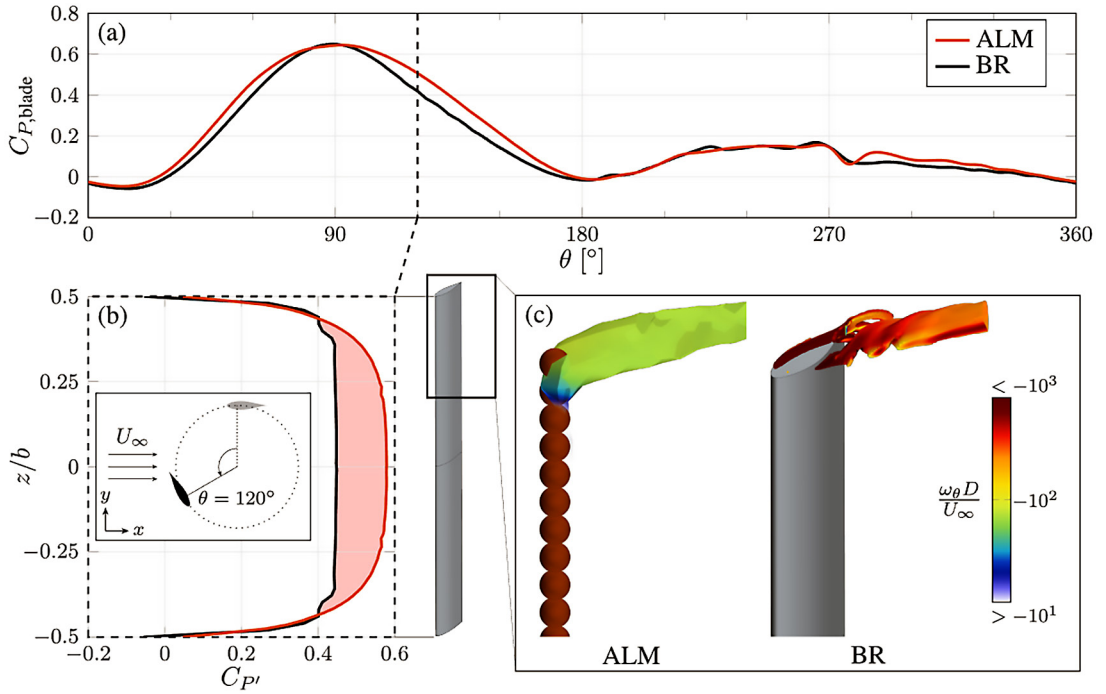

Figure 8: Graphical illustration for the overprediction of the power with the ALM. (a) Evolution of C_P of one blade over a turbine revolution. (b) Spanwise distribution of the section power coefficient ($C_{P'}$) along a blade at $\theta = 120°$. (c) Isosurface of the Q-criterion coloured with tangential vorticity (ω_θ), representing the tip vortex generated by the Blade-Resolved (BR) and Actuator Line Method (ALM) turbines.

mainly in the upstream phase of rotation (θ ϵ [0°, 180°]), especially around the angular position $\theta = 120°$. At such positions, the ALM overpredicts the spanwise distribution of the blade's section power coefficient $C_{P'}$ mostly at the mid-span region of the blade, which is highlighted with red shaded area in Figure 8b. These discrepancies are related to 3D aerodynamic effects, which are revealed through the comparison of the tip vortices shown in Figure 8c. The tip vortex generated by the ALM exhibits a larger core with significantly lower vorticity than that in the BR simulation. This leads to a reduced downwash along the blade span, a phenomenon also reported by Breault et al. [31]. With a weaker downwash induced by the ALM's tip vortices, abnormally larger effective angles of attack (α) are perceived around the mid-span. As a result, the tangential force on the blade generated by the lift-drag combination (and therefore C_P) is overestimated. This occurs because the volumetric forces implemented in the fluid domain extend beyond the actual blade thickness (i.e., a larger force spreading). As mentioned in Breault et al. [31], using a smaller spreading of the volumetric forces in the thickness direction of the blade could generate stronger tip vortices. This would involve unsymmetric Gaussian smoothing of the applied volumetric forces. This is out of the scope of the present work and has been rejected.

This issue does not arise with the EPTM since it is constructed using global turbine performance metrics extracted from a representative BR simulation. Considering that the ALM's overprediction of power is considered to be systematic, a simple ad hoc

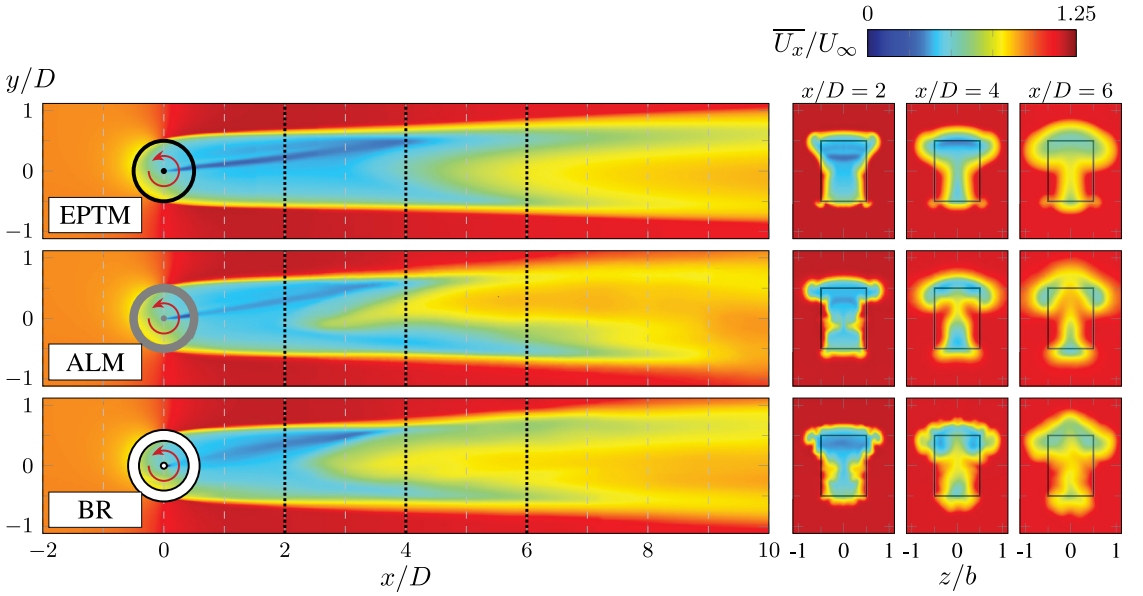

Figure 9: Comparison of the mean wake for the single turbine scenario (#1) generated by the three turbine modelling approaches through contours of mean streamwise velocity from a top view on the mid-span plane section (left) and a cross-section view at x/D = 2, 4, and 6 (right). Rectangles on the cross-section view represent the projection of the turbine extraction plane on the cross section.

correction is proposed based on the relative difference in the maximum mean power of the isolated turbine (at $\lambda_{opt} = 3$) between the ALM and the BR simulations:

$$\left(\overline{C_P}\right)_{\text{ALM}}^{\text{corr}} = \frac{\left(\overline{C_P}\right)_{\text{opt, BR}}}{\left(\overline{C_P}\right)_{\text{opt, ALM}}} \cdot \left(\overline{C_P}\right)_{\text{ALM}}$$

$$\approx 0.87\left(\overline{C_P}\right)_{\text{ALM}}. \quad (8)$$

The corrected $\overline{C_P}$ curve of the ALM shows improved agreement with the curve derived from the BR simulations, as shown in Figure 7a. This ad hoc correction will be systematically used for all the ALM power predictions in this work.

In addition to the performance prediction, the wake reproduction is also a key capability of a turbine model, which may affect significantly the performance prediction accuracy for downstream turbines in array deployments. Figure 9 compares the mean wake generated by the EPTM and the ALM with that of the reference BR simulation through mean streamwise velocity contours, confirming that the characteristic wake topology is reasonably well reproduced by both simplified models. The wakes are all found to be deflected transversely toward the positive y direction (i.e., toward the upper part of rotation ($\theta \in$ [-90˚, 90˚])) and contracted in the spanwise (z) direction, forming a similar T-shaped deficit viewed on downstream cross-section planes. The rapidly recovered centre zone, observed from 2D downstream of the ALM and BR rotors, but only from 4D downstream of the EPTM, is effectively attributed to this wake deformation. In fact, it has been previously proved by Boudreau and Dumas [32] that the convection of the mean flow contributes predominantly to the wake recovery along the centreline.

Wake recovery could be globally estimated with the space-averaged mean streamwise velocity on successive wake plane sections,

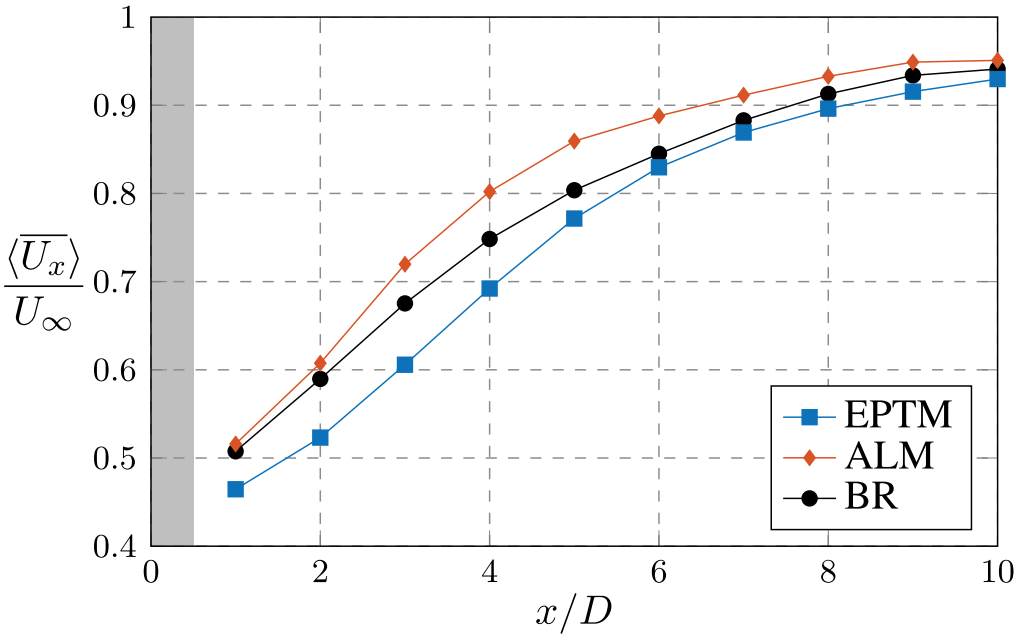

Figure 10: Streamwise evolution of the section-averaged mean streamwise velocity in the wake of the Effective Performance Turbine Model (EPTM), Actuator Line Method (ALM), and Blade-Resolved (BR) rotors. The streamwise extent of the turbine sweeping region is shaded in grey.

which are aligned with the turbine extraction plane and geometrically identical. This section-averaging operation is denoted by angle brackets (‹·›). As shown in Figure 10, the ALM's mean wake shares comparable recovery rate with that of the BR rotor in the near-wake region ($0 < x/D < 3$), owing to the correctly predicted spanwise contraction, which itself is induced by the blade's tip vortices. Its overly rapid recovery around $4D$ – $5D$ downstream is supposed to be attributed to the overpredicted transverse convection toward $+y$.

The EPTM wake shows slower recovery in the near-wake region due to a spanwise contraction less pronounced. Nonetheless, in the far-wake zone ($x/D > 6$), which exhibits higher potential for downstream aligned turbine deployment, the mean wake profiles regenerated by the two simplified approaches match well that of the BR turbine, with a relative difference in $\langle\overline{U_x}\rangle$ lower than 5% for the ALM and 2% for the EPTM.

4.2 Scenario #2: Tandem Array

In the tandem scenario, a second turbine (T2) is placed $6D$ downstream of the first turbine (T1), as illustrated in Figure 5b. The domain retains the same cross section as in scenario #1; thus, the blockage ratio of the two turbines remains $B = 20\%$.

As the longitudinal spacing between the turbines is sufficiently large, it is reasonable to assume that the ambient flow conditions of the upstream turbine T1 are unaffected by the turbine T2. With the same blockage ratio and inflow conditions as in the single turbine scenario, it is expected that the optimal tip-speed ratio of the T1 is unchanged (i.e., $\lambda_{\mathrm{opt,T1}} = 3$). However, as the turbine T2 operates in the T1's wake flow, which is not fully recovered, its inflow should be slower than the reference velocity U_∞, and thus $\lambda_{\mathrm{opt,T2}}$ is anticipated to be lower than 3. Through manual tuning in the BR simulation, it was

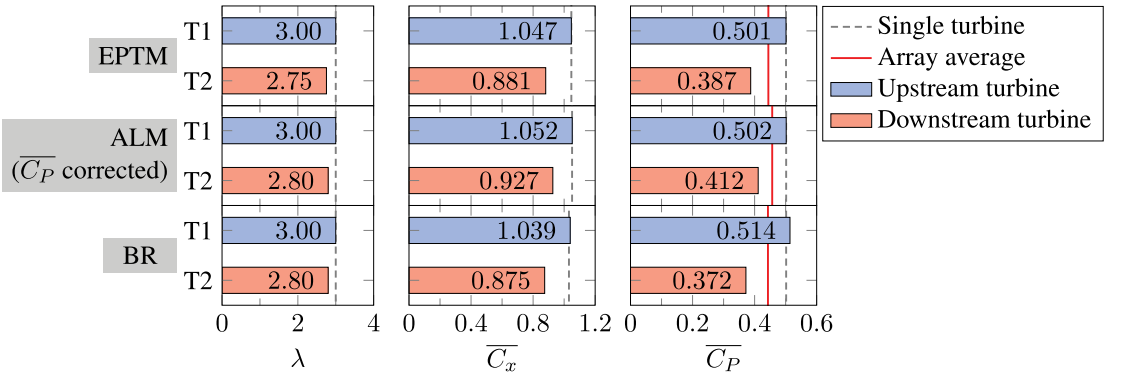

Figure 11: Mean performance prediction for each turbine in the tandem array scenario (#2) from different turbine modelling approaches. For the Actuator Line Method (ALM) simulation, the power correction (Equation (8)) is applied. The grey dashed lines represent the performances of the single turbine (scenario #1) as reference. The red solid lines indicate the mean power coefficient averaged across the array.

indeed confirmed in a previous study that $\lambda_{opt,T2} = 2.8$ [6]. These values of $\lambda_{opt,T1}$ and $\lambda_{opt,T2}$ were prescribed for the BR and ALM simulations, which align well with the optimal tip-speed ratios auto-detected by the EPTM ($\lambda_{opt,T1} = 3$ and $\lambda_{opt,T2} = 2.75$, see Figure 11).

Predictions of the mean drag and power coefficients within the array are presented in Figure 11 as well. For the upstream turbine T1, the mean drag and power coefficients remain unchanged compared to the values of the single turbine at its optimal operating point (see Figure 7), confirming the fact that the influence of T2 on T1 is negligible. One may observe minor discrepancies between the T1 and the single turbine in the BR simulations, which are probably attributed to the slight differences in mesh resolution adopted in the two scenarios #1 and #2.

The mean drag and power of the downstream turbine T2 are respectively reduced by 16% and 28% compared to T1, as predicted by the reference BR simulation, which is not surprising since T2 encounters the slower incoming flow from T1 with lowered momentum and power flux than the free stream. This trend is correctly reproduced by both simplified models (see Figure 11). The T2's actuating lines (i.e., the ALM blades), dynamically acting as real solid blades, perceive non-uniformly decelerated effective local freestream velocity V along the blade trajectory, and generate overall lower forces over the revolution (through Equations (6) and (7)), leading to a reduced power prediction. More precisely, as shown in Figure 12, the ALM predicts an instantaneous blade power reduction comparable to the BR prediction, occurring primarily in the upstream phase of rotation and with similar peak values, not exactly at the same moment in the cycle (at the angular position of 90° for ALM and 105° for BR). By contrast, the EPTM works in a more averaged but robust way: a lower effective velocity is computed on the T2's extraction plane ($V^*_{T2} < V^*_{T1}$), yielding consistently decreased value of forces and power. The differences in the performance prediction across the three approaches are found to be greater for T2 than for T1, which is caused by the discrepancy in upstream wake reproduction. The EPTM and the ALM overpredicts the drag of T2 by 0.8% and 6%, and the power by 4% and 11%, respectively,

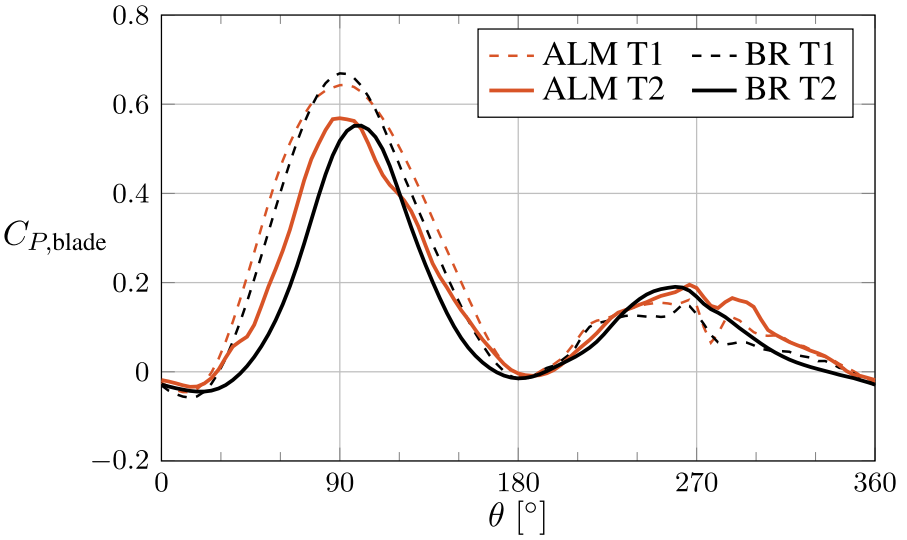

Figure 12: Evolution of C_P of one blade for both turbines in the tandem array scenario (#2), predicted by both unsteady turbine modelling approaches Actuator Line Method (ALM) and Blade-Resolved (BR).

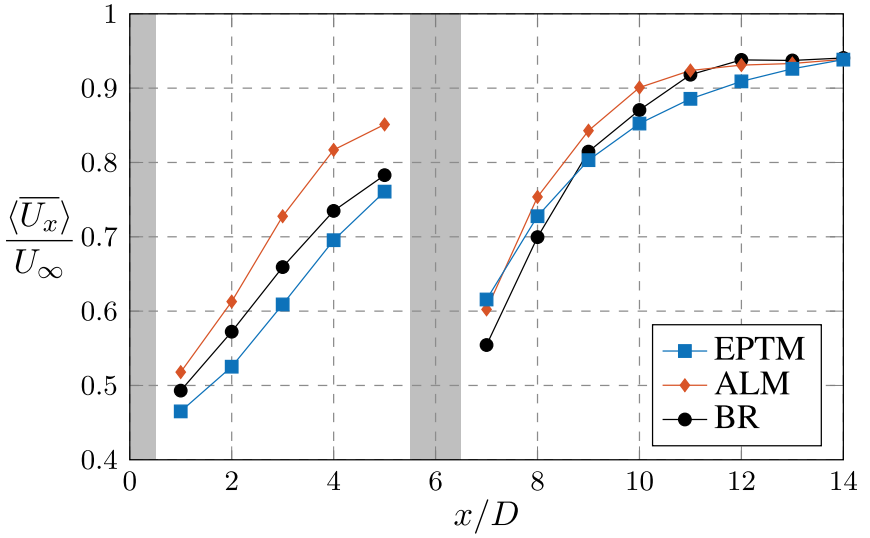

Figure 13: Streamwise evolution of the section-averaged mean streamwise velocity for the tandem array scenario (#2) predicted by the three turbine models. The shaded zones correspond to the streamwise extent occupied by the rotors.

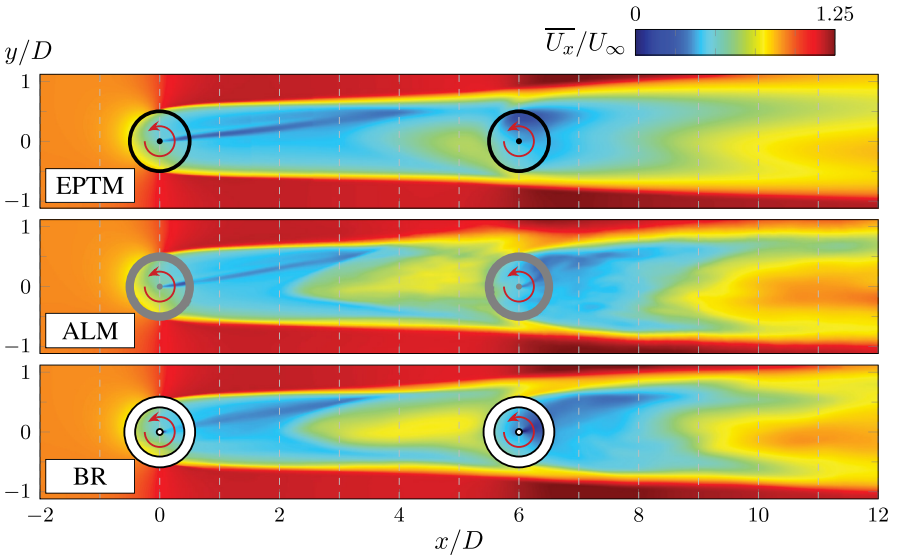

Figure 14: Comparison of the mean wake for the tandem array scenario (#2) generated by the three turbine modelling approaches through contours of mean streamwise velocity on the mid-span plane section.

compared to the BR simulation. Nonetheless, the performance predictions of the simplified models can still be considered consistent to the reference values obtained in the BR simulation, falling into acceptable difference ranges.

Figure 13 and Figure 14 compare the wake recovery for the three simulations of scenario #2. It is found that the T1's wake, almost unaffected by the T2 up to 1D upstream of T2 (i.e., $x/D \leq 5$), shows discrepancies among the three approaches as was noticed for the single turbine (see Section 4.1), which strongly affect the performance prediction accuracy for T2. In fact, the overprediction of power (after correction) of the ALM T2 is related to the excessively recovered upstream wake. Moreover, the fact that the upstream wake recovering centre of the ALM rotor is more toward the positive y direction than that of the BR rotor (as illustrated in the right panels of Figure 9 for $x/D = 4$ and 6) explains the prediction difference for the angular position of the blade extraction peak viewed in Figure 12. Conversely, even with an underestimated inflow velocity, the EPTM overpredicts slightly the power for T2. This arises from the large non-uniformity of the incoming flow in this case, since the EPTM is developed from a single turbine operating in uniform flow, not accounting for the turbine power reduction in wake flows. From another perspective, the EPTM may perform better in other array configurations where one would want to avoid severely sheared inflow for the downstream turbines. The T2's mean wake regenerated by the two simplified models resembles quite closely the mean wake of the BR rotor (see Figure 13 and Figure 14), meaning that the performance prediction accuracy would be good for hypothetic turbines deployed further downstream in the wake.

4.3 Scenario #3: Triangular Cluster

The third scenario consists of three turbines configured into a triangular (staggered) cluster. As illustrated in Figure 5c, two counter-rotating turbines (T1 and T2) are placed side by side with a lateral spacing of 2.24D at $x/D = 0$ into a channel maintaining a constant blockage ratio of 20%. Another turbine (T3) is positioned downstream along the midline between the upstream turbines. Configurations with various longitudinal spacings (s_x) from 1.2D to 6D and two rotation patterns (named "inward" and "outward," as illustrated in Figure 15) are tested using the EPTM. With lateral symmetric planes present, these configurations are practically equivalent to two-row arrays of infinite width, where side-by-side turbines rotate in alternating directions. ALM simulations are conducted only for the best and worst cases predicted by the EPTM simulations (i.e., with the highest and lowest average power extraction). However, high-fidelity BR simulations are not conducted in this triangular cluster scenario since it becomes too expensive.

As expected, the EPTM predicts always an optimal tip-speed ratio close to 3 for the upstream turbines T1 and T2 since their inflow and blockage conditions remain unchanged compared to scenario #1. Larger optimal tip-speed ratios are predicted for T3, with $\lambda_{opt,T3}$ ranging from 3.15 to 3.25 depending on turbine arrangements.

As shown in Figure 16, the EPTM predicts a decreasing trend in the mean power extraction with increasing longitudinal spacing; however,

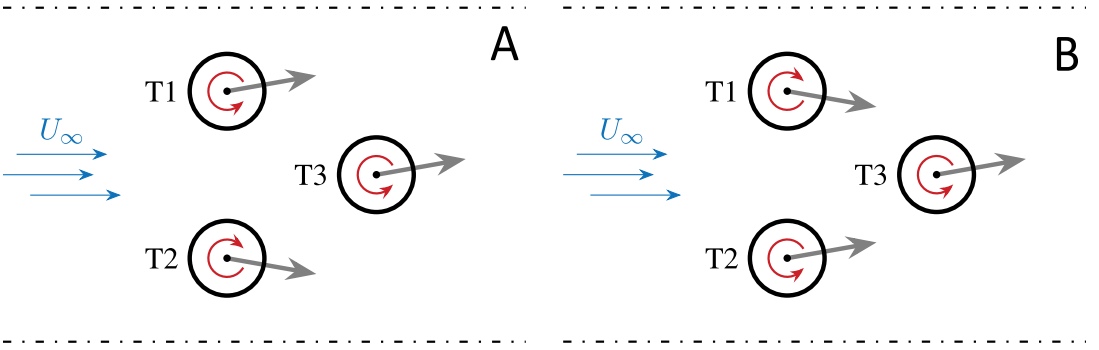

Figure 15: Test configurations of turbine rotation direction in triangular clusters illustrated from top view by red arrows. The grey arrows indicate the anticipated wake deflection direction of each turbine. (a) Inward rotation. (b) Outward rotation.

the cluster average is always higher than the single turbine's mean power. This array performance improvement is attributed to the accelerated bypass flow between the turbines T1 and T2 hitting the turbine T3. In these test configurations, T3 extracts about 10% – 25% more power than the average of the upstream turbines, while the average power production of the upstream row remains quite close to that of the single turbine. The impact of the rotation direction is limited in this case. For the most compact configurations, the inward-rotating upstream turbines produce more power than the outward-rotating ones, whereas this effect diminishes when s_x exceeds $2D$.

For configurations with $s_x/D > 4$, upstream turbines rotating outward (with upstream wakes defecting inward) are more detrimental to T3's power extraction. These above trends jointly determine the best- and worst-performing cases, i.e., the $s_x/D = 1.2$ configuration with inward rotation and the $s_x/D = 6$ configuration with outward rotation, respectively. The two cases are now investigated in more detail and compared with the ALM simulations.

The most pronounced discrepancy between the two cases lies in the performance of the downstream turbine T3. The ALM's power predictions are quite consistent to those of the EPTM (about 1% of difference), except for the downstream turbine T3 in the worst case (9% of difference), as presented in the right panels of Figure 17.

In the best cases, T3 benefits from the accelerated bypass flow between the upstream turbines, resulting in a notably enhanced mean power $\overline{C_{P,\mathrm{T3}}}$ (+25 relative to the single turbine scenario, as predicted by both EPTM and ALM). As predicted by the ALM, the benefit to the blade instantaneous power extraction occurs mainly in the upstream phase of rotation, while the effect on the downstream phase is quite limited (see Figure 18).

In the worst case, the EPTM predicts a much less increase in $\overline{C_{P,\mathrm{T3}}}$ (+13%), whereas the ALM predicts that there is only a small gain of 3% for T3. For one thing, this reduced gain for T3 results from the gradually decelerated bypass flow with the reenergization of the upstream wakes, which explains also the power reduction of T3 with increasing longitudinal spacing as observed in Figure 16. This is further supported by the observation in Figure 18 that the maximum $C_{P,\mathrm{blade}}$ in the worst case, while lower than that in the best case, still exceeds that of

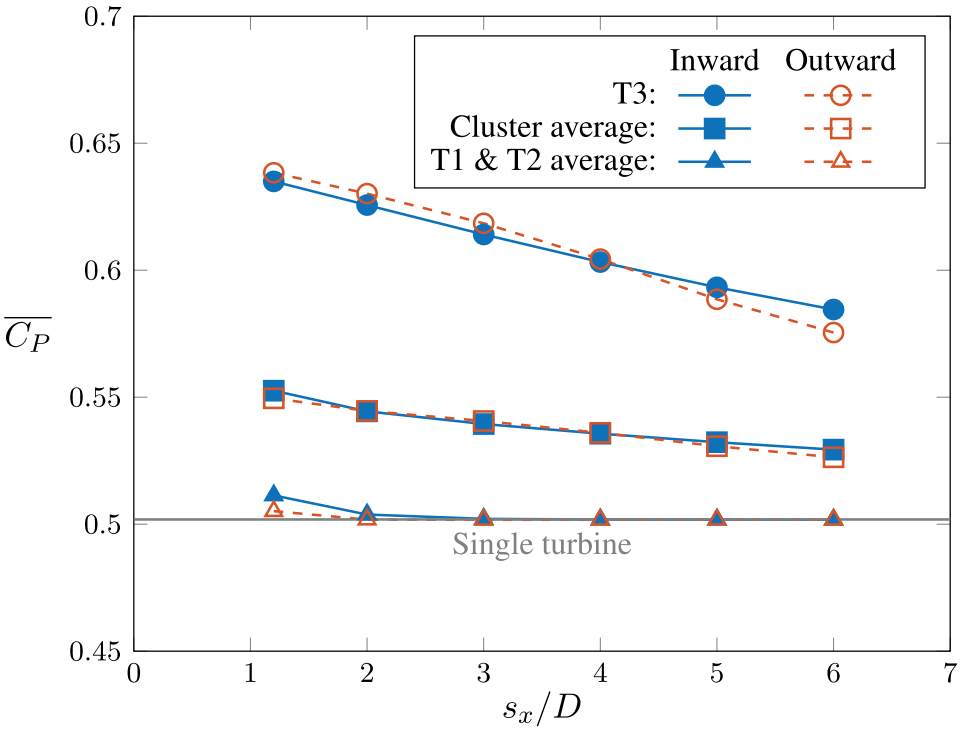

Figure 16: Mean power coefficient $\overline{C_P}$ for the triangular cluster with different longitudinal spacing s_x and rotation patterns, as predicted by the Effective Performance Turbine Model (EPTM).

a single turbine, as predicted by the ALM. For another, in the worst case, due to the inward deflection of the upstream wakes, the velocity deficit penetrates the T3's extraction region (as viewed on the left panels of Figure 17b for both the EPTM and ALM), causing notable wake-turbine interaction and performance degradation for T3, which is also revealed by a decrease in instantaneous power extracted by the single blade around $\theta = 45^\circ$ and 150° (see Figure 18); by contrast, this detrimental effect is well avoided in the best case. The discrepancy between the two approaches in the power prediction of T3 is not such a surprise since the ALM's wake is more diffused, resulting in a slower bypass and a stronger penetration of velocity deficit into the T3's extraction region.

Moreover, minor differences are noted for the two upstream turbines in the compact cluster (best case) compared to the single turbine scenario, which may be marginal for array deployment studies yet meaningful for the purpose of model comparison. Firstly, the upstream turbines, on average, extract 2% more power than the single turbine. Since T3 is placed downstream between the two upstream turbines at a sufficiently short distance, the blockage effect of the upstream row is effectively enhanced by the presence of the closely placed downstream row. Secondly, both EPTM and ALM predict that T1 extracts 6% less power than T2 in the best (compact) configuration, which is caused by the asymmetric upstream deceleration (visible right upstream of T3 in Figure 17 (left)) induced by T3.

In brief, the two simplified turbine models are not only able to predict similar trends in the mean power variation across the clusters in a

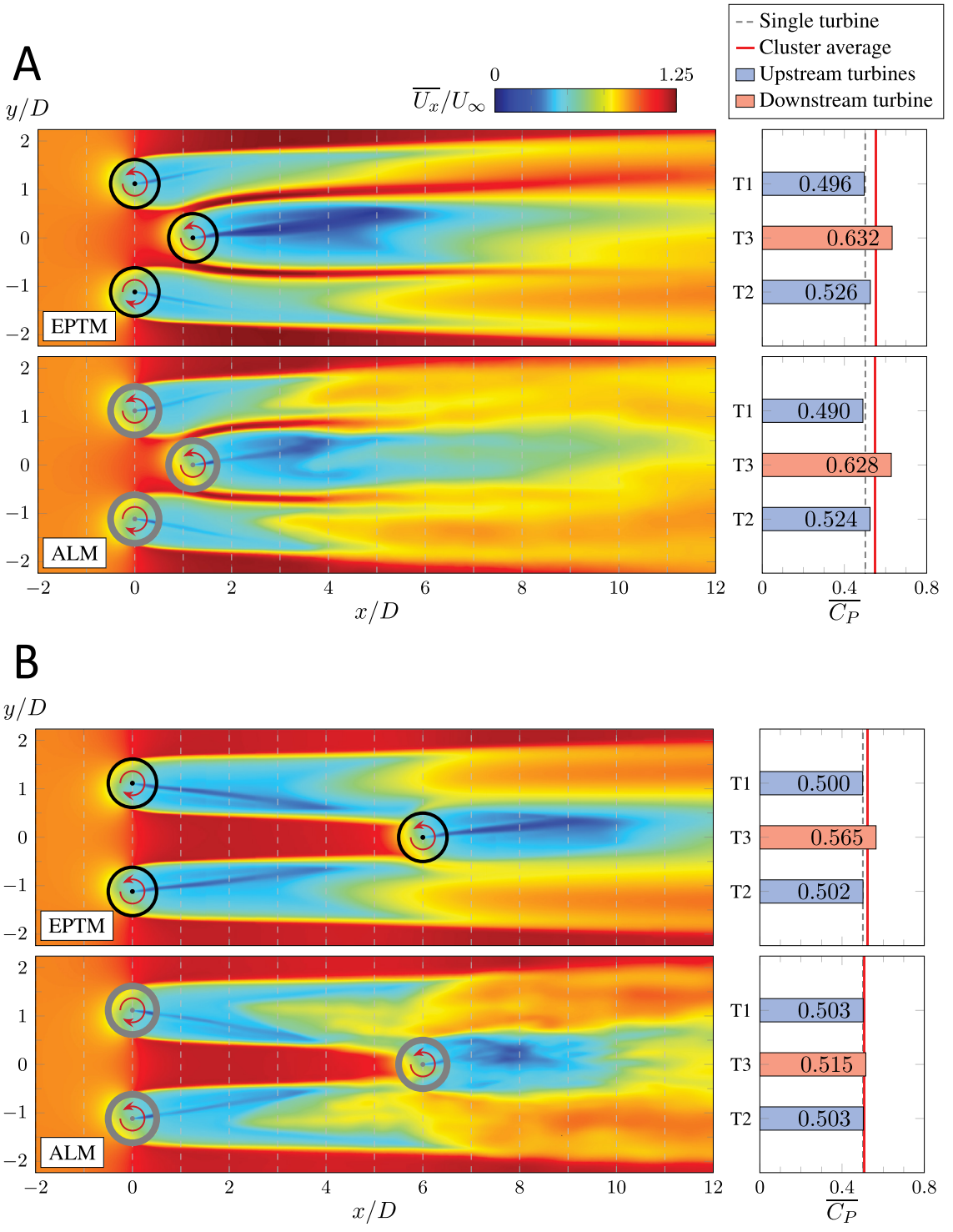

Figure 17: Comparison of the mean wake produced (top) and the mean power prediction (bottom) of the Effective Performance Turbine Model (EPTM) versus Actuator Line Method (ALM) for the two triangular clusters with the best and worst performances. Mean streamwise velocity are shown on the mid-span plane section. (a) Best case: s_x/D = 1.2, inward rotation. (b) Worst case: s_x/D = 6, outward rotation.

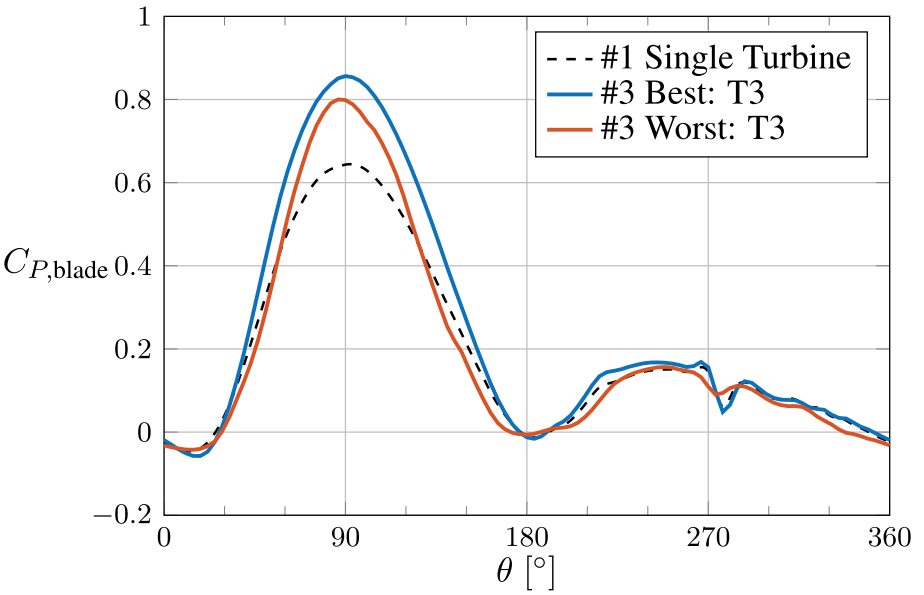

Figure 18: Evolution of C_P of one blade for the downstream turbine T3 in the triangular array scenario (#3), in comparison to the single turbine scenario (#1).

simple manner, but can also reproduce consistent flow phenomena and effects (even minor ones) associated with these observed trends.

4.4 Computational Costs

A comparison of the computational costs required by the three turbine modelling approaches is provided in Figure 19. The EPTM and ALM simulations employ comparable mesh cell counts, roughly five million cells per turbine, which is of the order of 10^{-1} of that used in the BR simulations. However, since the EPTM is a steady-state model, which does not require temporal marching nor time statistics for mean turbine performance, its has always the lowest Central Processing Unit (CPU) time requirement among the three methods. The CPU hour consumption of the EPTM grows with the cell count and also with the complexity of interactions within the turbine array which may require more iterations to converge. For comparison purposes, the CPU time requirements of the two unsteady methods ALM and BR shown in Figure 19 are estimated according to a conservative scenario. It is supposed that a minimum of ten turbine cycles discretized with 360 steps/cycle and five final cycles in 1,000 steps/cycle are required for the single turbine scenario (#1) and the compact triangular cluster (#3 best). Ten more coarsely discretized cycles are required before the final cycles for the tandem array scenario (#2) and the extended triangular cluster (#3 worst) so that the wake from the upstream turbines could be effectively transported to the turbine located far downstream. The ALM consumes on average about 2×10^4 CPU hours per turbine, equivalent to five days of computation on a 192-core compute node, being approximately 1,000 times more than the EPTM demand; nonetheless, the ALM is still about five times faster than the high-fidelity BR simulation.

5. CONCLUSION

This study presented a comparative assessment of two simplified turbine models

(EPTM and ALM) tailored for CFTs. Their performance prediction, wake reproduction, and computational costs were evaluated with three deployment scenarios to determine each model's suitability for turbine farm simulations.

The EPTM was shown to accurately predict the performance of each scenario, with the only minor discrepancy being a slower wake recovery in the near wake, as demonstrated by comparisons with blade-resolved results for the first two scenarios. The main advantage of this method lies in its low computational costs. In fact, it is considerably more cost-effective: $\sim 10^3$ times less CPU hours than the ALM simulations, making it an efficient alternative to unsteady models and ideally suited for large-scale turbine farm simulations. Indeed, this model could be applied to farms with more than 20 turbines while maintaining excellent accuracy in the predicted results.

The ALM was shown to effectively reproduce the overall performance trends and the wake due to its unsteady modelling approach. A systematic correction based on the relative difference in the mean power coefficient of the single turbine scenario was developed to mitigate the overprediction of the C_P. This correction notably enhanced the predictive capability of the ALM. However, the corrected ALM still exhibited a slight overprediction compared with the EPTM, particularly for the downstream turbine in tandem configuration, due to the ALM faster wake recovery. In future work, such a correction could be derived from the flow physics observed in BR simulations (e.g., increased downwash from tip vortices). With this adjustment applied to its performance prediction, the ALM becomes more suitable for simulating small and compact turbine clusters (involving fewer than five turbines to maintain a reasonable computational cost) where near-wake interactions are strong and unsteady effects important.

Future work could focus on comparing and analyzing the models in the context of resource-turbine interactions by modifying the channel bed topography, including a free-surface model, and varying the flow turbulence level to assess the models under more realistic conditions representative of a river or tidal environments.

ACKNOWLEDGMENT

The authors thank the Digital Research Alliance of Canada for providing computational resources, as well as their colleagues at the LMFN especially Sébastian Bourget and Olivier Gauvin-Tremblay, Professor G. Winckelmans of Université catholique de Louvain, and Mr. J. Huang of Natural Resources Canada for all the fruitful discussions.

Authors' Declaration

- Funding: Financial support from the Natural Sciences and Engineering Research Council of Canada (NSERC Discovery Grant No. RGPIN-2024-06374; CGRS M Scholarship) and the Fonds de recherche du Québec (FRQNT BRE Scholarship) is gratefully acknowledged.
- Ethical approval: This paper does not contain any studies with human participants or animals.
- Competing interests: The authors declare that there are no competing interests.
- Availability of data and materials: Datasets used and/or analyzed during the current

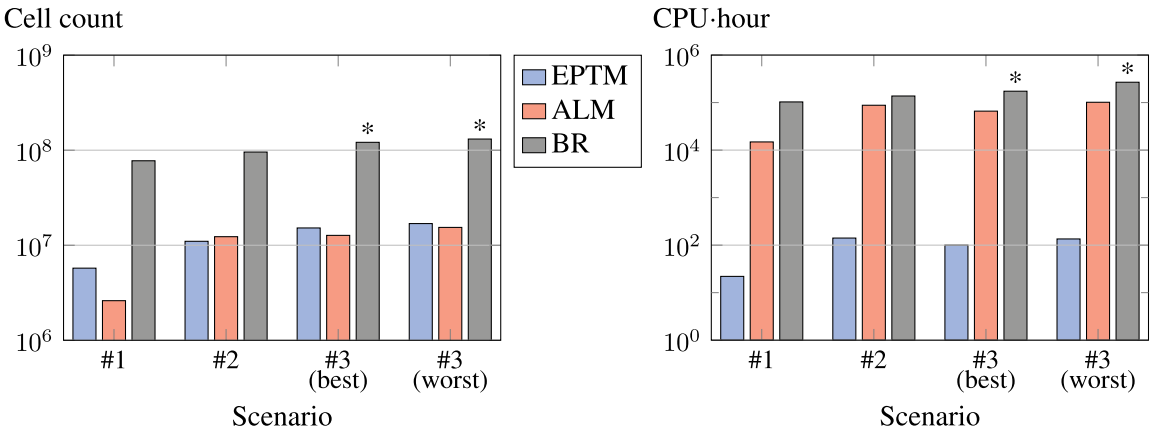

Figure 19: Comparison of the computational costs required by each turbine modelling approaches in terms of mesh cell count (top) and Central Processing Unit (CPU) time (bottom). Cases marked with an asterisk (*) were not performed; the corresponding costs are roughly estimated based on other cases.

study are available from the corresponding author upon reasonable request.

- Artificial intelligence: During the preparation of this work the authors used the ChatGPT tool as a writing assistant, particularly for translation, paraphrasing, as well as spelling and grammar correction. After using this tool, the authors reviewed and edited the content as needed and take full responsibility for the content of the publication.

REFERENCES

[1] I. Paraschivoiu, *Wind Turbine Design: With Emphasis on Darrieus Concept*. Montréal, QC, Canada: Polytechnic International Press, 2002.

[2] D. De Tavernier, C. Ferreira and A. Goude, "Vertical-axis wind turbine aerodynamics," in *Handbook of Wind Energy Aerodynamics*, Cham, Switzerland: Springer Nature, 2022, pp. 1-45.

[3] J. O. Dabiri, "Potential order-of-magnitude enhancement of wind farm power density via counter-rotating vertical-axis wind turbine arrays," *Journal of Renewable and Sustainable Energy*, vol. 3, p. 043104, 2011. doi: 10.1063/1.3608170.

[4] T. Nishino and R. H. Willden, "Two-scale dynamics of flow past a partial cross-stream array of tidal turbines," *Journal of Fluid Mechanics*, vol. 730, pp. 220-244, 2013. doi: 10.1017/jfm.2013.340.

[5] O. Gauvin-Tremblay and G. Dumas, "Hydrokinetic turbine array analysis and optimization integrating blockage effects and turbine-wake interactions," *Renewable Energy*, vol. 181, pp. 851-869, Jan. 2022. doi: 10.1016/j.renene.2021.09.003.

[6] O. Gauvin-Tremblay and G. Dumas, "A numerical study on the interaction between two cross-flow turbines in tandem configuration to support a simplified turbine model approach," *Journal of Renewable and Sustainable Energy*, vol. 12, no. 5, p. 054502, Sep. 2020. doi: 10.1063/5.0018237.

[7] S. Draper and T. Nishino, "Centred and staggered arrangements of tidal turbines," *Journal of Fluid Mechanics*, vol. 739, no. 1, pp. 72-93, Mar. 2014. doi: 10.1017/jfm.2013.593.

[8] T. Kinsey and G. Dumas, "Impact of channel blockage on the performance of axial and cross-flow hydrokinetic turbines," *Renewable Energy*, vol. 103, pp. 239-254, Apr. 2017. doi: 10.1016/j.renene.2016.11.021.

[9] J. I. Whelan, J. M. R. Graham and J. Peiró, "A free-surface and blockage correction for tidal turbines," *Journal of Fluid Mechanics*, vol. 624, pp. 281-291, Apr. 2009. doi: 10.1017/S0022112009005916.

[10] L. Kuang, H. Lei, D. Zhou, Z. Han, Y. Bao and Y. Zhao, "Numerical Investigation of Effects of Turbulence Intensity on Aerodynamic Performance for Straight-Bladed Vertical-Axis Wind Turbine," *Journal of Energy Engineering*, vol. 147, no. 1, p. 04020087, Feb. 2021. doi: 10.1061/(ASCE)EY.1943-7897.0000740.

[11] A. Talamalek, M. C. Runacres and T. De Troyer, "Effect of Free-Stream Turbulence on the Power Performance and Wake Characteristics of Paired Counter-Rotating Vertical-Axis Wind Turbines," *Wind Energy*, vol. 28, no. 2, pp. 1-25, Feb. 2025. doi: 10.1002/we.2968.

[12] J. Thiébot, N. Guillou, S. Guillou, A. Good and M. Lewis, "Wake field study of tidal turbines under realistic flow conditions," *Renewable Energy*, vol. 151, pp. 1196-1208, May 2020. doi: 10.1016/j.renene.2019.11.129.

[13] T. Villeneuve, M. Boudreau and G. Dumas,

"Improving the efficiency and the wake recovery rate of vertical-axis turbines using detached end-plates," *Renewable Energy*, vol. 150, pp. 31-45, May 2020. doi: 10.1016/j.renene.2019.12.088.

[14] T. Villeneuve, G. Winckelmans and G. Dumas, "Increasing the efficiency of vertical-axis turbines through improved blade support structures," *Renewable Energy*, vol. 169, pp. 1386-1401, May 2021. doi: 10.1016/j.renene.2021.01.092.

[15] R. Gosselin, "Analysis and optimization of vertical axis turbines," PhD thesis, Department of Mechanical and Industrial Engineering, Université Laval, Québec City, QC, Canada, 2015.

[16] S. Bourget, "Development and assessment of a modeling method for hydrokinetic turbines operating in arrays," M.Sc. thesis, Department of Mechanical and Industrial Engineering, Université Laval, Québec City, QC, Canada, 2018. [Online]. Available: https://hdl.handle.net/20.500.11794/31588

[17] P. Rochefort, "Modélisation aéro-hydrodynamique de turbines à axe vertical H-Darrieus (VAT) par la méthode des lignes actuatrices (ALM) et caractérisation des effets de courbure," M.Sc. thesis, Department of Mechanical and Industrial Engineering, Université Laval, Québec City, QC, Canada, 2025. [Online]. Available: https://hdl.handle.net/20.500.11794/178663

[18] S. Bourget, O. Gauvin-Tremblay and G. Dumas, "Hydrokinetic turbine array modeling for performance analysis and deployment optimization," *Transactions of the Canadian Society for Mechanical Engineering*, vol. 42, no. 4, pp. 370-381, Jul. 2018. doi: 10.1139/tcsme-2017-0088.

[19] P. Bachant and M. Wosnik, "Effects of Reynolds Number on the Energy Conversion and Near-Wake Dynamics of a High Solidity Vertical-Axis Cross-Flow Turbine," *Energies*, vol. 9, no. 2, p. 73, Feb. 2016. doi: 10.3390/en9020073.

[20] O. Gauvin-Tremblay, "Modeling and optimizing hydrokinetic turbine arrays using numerical simulations," PhD thesis, Department of Mechanical and Industrial Engineering, Université Laval, Québec City, QC, Canada, 2021.

[21] R. Merabet and É. Laurendeau, "Hovering Helicopter Rotors Modeling Using the Actuator Line Method," *Journal of Aircraft*, vol. 59, no. 3, pp. 774-787, May 2022. doi: 10.2514/1.C036314.

[22] F. Trigaux, P. Chatelain and G. Winckelmans, "Investigation of blade flexibility effects on the loads and wake of a 15 MW wind turbine using a flexible actuator line method," *Wind Energy Science*, vol. 9, no. 8, pp. 1765-1789, Aug. 2024. doi: 10.5194/wes-9-1765-2024.

[23] R. J. Stevens, L. A. Martínez-Tossas and C. Meneveau, "Comparison of wind farm large eddy simulations using actuator disk and actuator line models with wind tunnel experiments," *Renewable Energy*, vol. 116, pp. 470-478, Feb. 2018. doi: 10.1016/j.renene.2017.08.072.

[24] M. J. Churchfield, S. J. Schreck, L. A. Martinez-Tossas, C. Meneveau and P. R. Spalart, "An Advanced Actuator Line Method for Wind Energy Applications and Beyond," in *AIAA 2017-1998. 35th Wind Energy Symposium*, Grapevine, TX, USA, Jan. 9-13, 2017. doi: 10.2514/6.2017-1998.

[25] G. Winckelmans, P. Rochefort, T. Villeneuve, F. Trigaux, M. Duponcheel and G. Dumas, "Improved modeling of flow curvature effects on vertical-axis turbines, and actuator line method with aerodynamic moment," *Wind Energy Sciences*, pre- print, Dec. 2025. doi: 10.5194/wes-2025-283.

[26] F. Trigaux, T. Villeneuve, G. Dumas and G. Winckelmans, "Near-tip correction functions for the actuator line method to improve the predicted lift and drag distributions," *Journal of Fluid Mechanics*, vol. 989, p. A1, Jul. 2024. doi: 10.1017/jfm.2024.461.

[27] P. Bachant, A. Goude and M. Wosnik, "Actuator line modeling of vertical-axis turbines," 2018, *arXiv: arXiv:1605.01449*.

[28] R. Zhao, A. C. W. Creech, A. G. L. Borthwick, V. Venugopal and T. Nishino, "Aerodynamic Analysis of a Two-Bladed Vertical-Axis Wind Turbine Using a Coupled Unsteady RANS and Actuator Line Model," *Energies*, vol. 13, no. 4 p. 776, 2020. doi: 10.3390/en13040776.

[29] P. F. Melani, F. Balduzzi, G. Ferrara and A. Bianchini, "Tailoring the actuator line theory to the simulation of Vertical-Axis Wind Turbines," *Energy Conversion and Management*, vol. 243, p. 114422, Sep. 2021. doi: 10.1016/j.enconman.2021.114422.

[30] Siemens Digital Industries Software, *Simcenter STAR-CCM+ version 2406*, 2024.

[31] M.-A. Breault, P. Rochefort and G. Dumas, "On the simulation of a wing with detached end-plates using an actuator line based on an anisotropic Gaussian kernel," *Transactions of the Canadian Society for Mechanical Engineering*, vol. 48, no. 4, pp. 534-542, Jan. 2024. doi: 10.1139/tcsme-2023-009.

[32] M. Boudreau and G. Dumas, "Comparison of the wake recovery of the axial-flow and cross-flow turbine concepts," *Journal of Wind Engineering and Industrial Aerodynamics*, vol. 165, pp. 137-152, June 2017. doi: 10.1016/j.jweia.2017.03.010.